JOURNAL OF COMPUTATIONAL PHYSICS **128,** 438–444 (1996)
ARTICLE NO. 0222

Finite-Element Models for Planar Hall Probes of Arbitrary Shape and Composition

STANLEY HUMPHRIES, JR.

Department of Electrical and Computer Engineering, University of New Mexico, Albuquerque, New Mexico 87131

Received September 6, 1995; revised March 28, 1996

Previous numerical models of planar Hall probes using finite-difference and finite-element methods were limited to open boundaries parallel to the coordinate axes. This paper derives the finite-element equations on a conformal triangular mesh directly from the law of current conservation. The treatment shows that the Hall condition for general curved boundaries is inherent in the equations and can be implemented in numerical programs with little effort. Results are presented from a code that can handle spatial variations of magnetic field, layer thickness, volume resistivity, and the Hall coefficient in probes of any shape.

1. INTRODUCTION

Semiconductor magnetic field sensors, or Hall-effect probes [1], have extensive applications in industry and research [2–4]. There is a substantial body of work on numerical modeling of probe characteristics using finite-difference equations and finite-element methods [5–14]. Because the finite-difference formulation is tied to the coordinate system, these models are constrained to simple geometries with boundaries parallel to the coordinate axes [15, 16]. Finite-element methods applied over conformal triangular meshes have removed this restriction in many areas of applied electromagnetism [17–20]. Although past finite-element treatments of Hall probes could address arbitrary variations of magnetic field and material properties through the material volume, the models were limited to straight Hall boundaries along the axes. The current paper shows that the Hall condition proceeds naturally from the finite-element equations and can be implemented easily on curved boundaries. The formulation allows mixed Dirichlet, Neumann, and Hall conditions on external or internal boundaries of any shape. Furthermore, the model can represent steady-state spatial variations of magnetic field, conductivity, Hall coefficient, and layer thickness.

In this paper, the finite-element equations for a planar Hall region are derived directly from the condition of current conservation over volumes surrounding each point of a triangular mesh. As an introduction, Section 2 reviews the finite-element equations for electrostatics that follow from a local application of Gauss's law. The approach is more direct than standard derivations using element shape functions and energy minimization [17]. In Section 3 the model is extended to include the effects of magnetic force. The law of current conservation leads to a set of linear equations that relate the potential of each mesh point to the values at neighboring points and the local injection current. The equations can be solved by matrix inversion or relaxation. Section 4 discusses implementation of the method in a computer code.

Figure 1 illustrates some design capabilities of the model. The computational region represents a thin layer of a homogenous *n*-type material with a 16.7° Hall angle. There are driving electrodes at the right and left boundaries. The circles at the top and bottom center are conducting contact pads. The triangles that constitute the mesh (Fig. 1a) conform to the material boundaries and allow enhanced resolution in the regions around the pads. Figure 1b shows equipotential lines of the solution with the pads connected to an open circuit. There is a smooth transition from the Dirichlet condition on the side boundaries to the Hall boundaries. The lines intersect open boundaries at the Hall angle, even in regions of strong curvature. Finally, Fig. 1c shows the effect of strong circuit loading between the pads, approximately halving the measured voltage.

2. FINITE-ELEMENT FORM OF POISSON'S EQUATION FROM GAUSS'S LAW

To introduce methods to treat Hall boundaries of a conductive medium, we shall first review the derivation of the familiar finite-difference equations for electrostatics using the Gauss' law approach of Refs. [21] and [22]. Consider the solution of the Poisson equation

$$\nabla \cdot (\varepsilon \nabla \phi) = -q. \tag{1}$$

In Eq. (1), the quantity ϕ is the electrostatic potential, ε is the spatially varying dielectric constant, and q is the space-charge density. The finite-difference approach represents the differential equation at a point by difference operators. In contrast, the finite-element method applies

0021-9991/96 $18.00

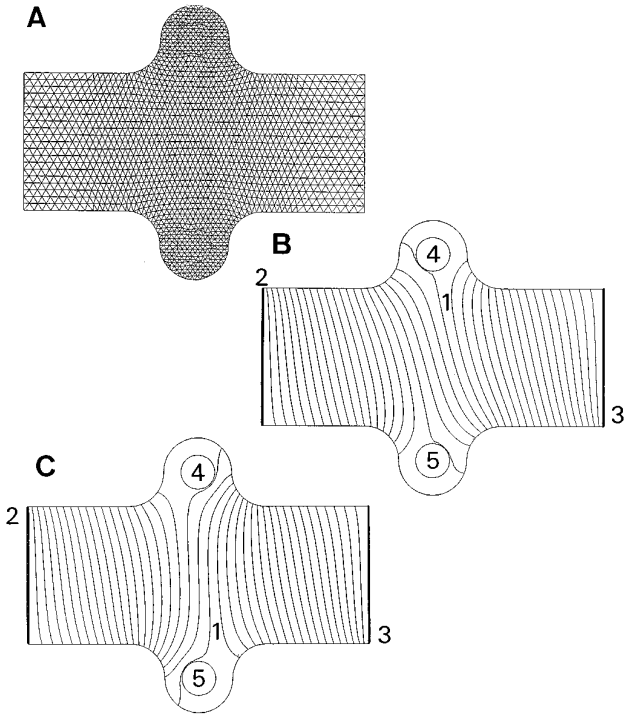

FIG. 1. Example, finite-element Hall probe model: height in y direction, 40 μm; length in x-direction, 100 μm; thickness, 1 μm; B_z, 100 G. Region 1, Conductive material with $K_h = -3.0 \times 10^{-4}$ V·cm/G·A, $\rho = 0.1\ \Omega \cdot$ cm; region 2, fixed potential, 0.0 mV; region 3, fixed potential, 10.0 mV; region 4, top sensor pad, $\rho = 0.005\ \Omega \cdot$ cm; region 5, bottom sensor pad, $\rho = 0.005\ \Omega \cdot$ cm. (a) Conformal triangle mesh with 3600 elements, (b) equipotential lines of solution (0.25 mV interval, with an open circuit between the sensor pads (Regions 4 and 5), (c) equipotential lines with 620 Ω load between the sensor pads.

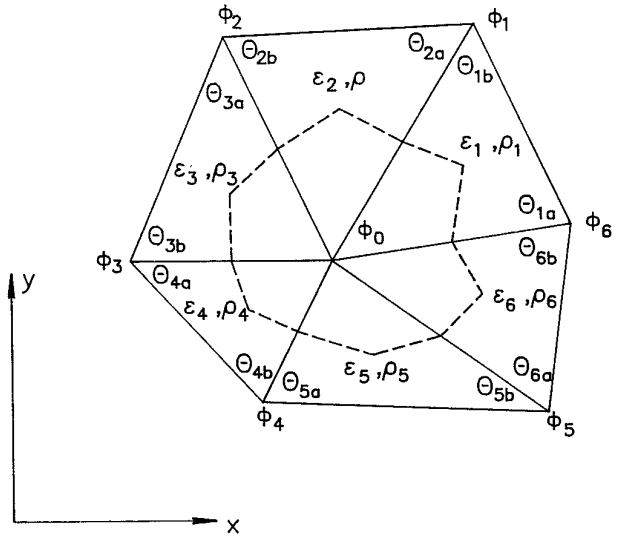

FIG. 2. Reference mesh vertex surrounded by six triangles and six neighboring vertices. Dashed line shows Gauss's law surface integration path.

integral relationships over small volumes of the solution space. The electrostatic equations follow from Gauss's law,

$$\iint \varepsilon \overline{E} \cdot \overline{dS} = \iiint q\, dV. \tag{2}$$

The electric field of Eq. (2) is related to the electrostatic potential by $\mathbf{E} = -\nabla\phi$. The quantity on the left is the integral of the normal electric field over a closed surface surrounding the volume indicated by the integral on the right-hand side.

Consistent with the planar Hall probe application, Eq. (2) will be applied to a two-dimensional geometry where quantities vary only in x and y. The computational region of the x–y plane is divided into triangular elements as in Fig. 1. The vertices of the triangles are called *mesh points* and the collection is called the *computational mesh.* Figure 2 shows a detail of a reference vertex surrounded by triangles defined by neighboring vertices. The point has six nearest neighbors. The following discussion can easily be extended to generalized meshes where points are surrounded with varying numbers of triangles. The reference numbers of the points and triangles are assigned in a positive rotational sense. The material quantities ε and q are taken as constant over the volume of each element. The electrostatic potential is approximated by a discrete function Φ defined at the vertices. A first-order treatment assumes a linear variation of potential over each element. The electric field is therefore constant in a triangle. To derive a difference equation relating the reference potential Φ_0 to neighboring values, Eq. (2) is applied around the dashed curve of Fig. 2 for a volume with height w in the z direction. The curve connects the midpoints of the lines between vertices to the mass centers of the elements. It therefore encloses one-third of the area of each triangle. We can immediately write an expression for the right-hand side of Eq. (2),

$$\sum_{i=1}^{6} \frac{q_i A_i w}{3}. \tag{3}$$

Here, the quantities A_i are the areas of the surrounding triangles in the x–y plane.

Evaluation of the surface integral (from Eq. (2) is more involved. To illustrate the method, consider the integral over the portion of the surface inside Triangle 2 of Fig. 2. Figure 3 shows the geometry of the triangle. For convenience, we define a coordinate system with origin at the reference vertex position. In this system, points 1 and 2 have the coordinates (x_1, y_1) and (x_2, y_2). The area of the triangle is

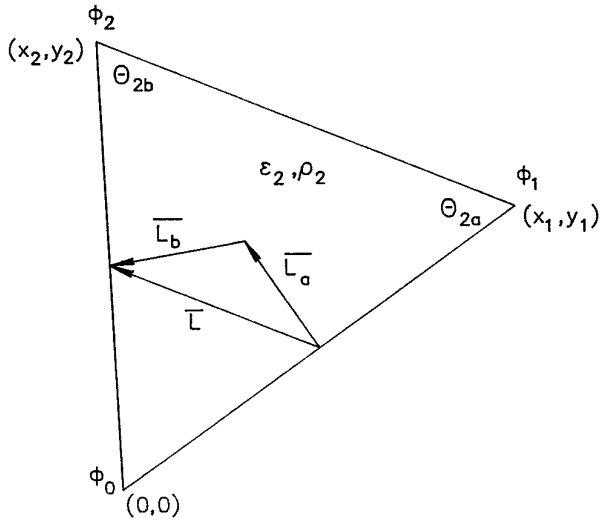

FIG. 3. Detailed view of Triangle 2 of Fig. 2, showing the Gauss's law surface integration path.

$$A_2 = \frac{(x_1 y_2 - x_2 y_1)}{2}. \tag{4}$$

The cotangents shown in the figure can be written in terms of the coordinates as

$$\cot\theta_{2a} = \frac{-y_1(y_2 - y_1) - x_1(x_2 - x_1)}{2A_2} \tag{5}$$

and

$$\cot\theta_{2b} = \frac{y_2(y_2 - y_1) + x_2(x_2 - x_1)}{2A_2}.$$

If the potential varies linearly over the triangle as

$$\phi_2(x, y) = \Phi_0 + ux + vy,$$

then the constant electric field in the triangle is

$$\overline{E_2} = u\bar{x} + v\bar{y}. \tag{6}$$

The constants in Eq. (6) are related to the vertex potentials and coordinates as

$$u = \frac{-\Phi_0(y_2 - y_1) + \Phi_1 y_2 - \Phi_2 y_1}{2A_2},$$
$$v = \frac{\Phi_0(x_2 - x_1) - \Phi_1 x_2 + \Phi_2 x_1}{2A_2}. \tag{7}$$

If **n** is a unit vector pointing outward from the surface of Fig. 2, the contribution to the Gauss's law integral from Triangle 2 can be written as

$$\iint \varepsilon_2 \overline{E_2}\cdot\bar{n}\, dS = \frac{w\varepsilon_2[(\overline{E_2}\times\overline{L_a}) + (\overline{E_2}\times\overline{L_b})]}{\bar{z}} = \frac{w\varepsilon_2(\overline{E_2}\times\overline{L})}{\bar{z}}. \tag{8}$$

The vectors $\mathbf{L}_a$, $\mathbf{L}_b$, and $\mathbf{L}$ are defined in Fig. 3. Inspection of the figure shows that the vector $\mathbf{L}$ is related to the vertex coordinates by

$$\overline{L} = \frac{(x_2 - x_1)}{2}\bar{x} + \frac{(y_2 - y_1)}{2}\bar{y}. \tag{9}$$

Substituting Eqs. (6), (7), and (9) into Eq. (8) gives the contribution from Triangle 2 as

$$\frac{\varepsilon_2 w[-\Phi_0(y_2 - y_1) + \Phi_1 y_2 + \Phi_2 y_1](y_2 - y_1)}{4A_2} - \frac{\varepsilon_2 w[-\Phi_0(x_2 - x_1) + \Phi_1 x_2 + \Phi_2 x_1](x_2 - x_1)}{4A_2}. \tag{10}$$

Equation (10) can be simplified using the coordinate-independent cotangent expressions of Eq. (5),

$$(w\varepsilon_2)[\Phi_0(\cot\theta_{2b} + \cot\theta_{2a}) - \Phi_1\cot\theta_{2b} - \Phi_2\cot\theta_{2a}]. \tag{11}$$

The full surface integral is the sum of Eq. (11) plus similar expressions for the other five triangles. Equating the result with the expression of Eq. (3) and solving for Φ_0 gives the following succinct form of Gauss's law:

$$\Phi_0 = \frac{\sum_{i=1}^{6} W_i\Phi_i + \sum_{i=1}^{6}(q_i A_i)/3}{\sum_{i=1}^{6} W_i}. \tag{12}$$

The coupling coefficients in Eq. (12) are given by

$$W_1 = \frac{(\varepsilon_2\cot\theta_{2b} + \varepsilon_1\cot\theta_{1a})}{2},$$
$$W_2 = \frac{(\varepsilon_3\cot\theta_{3b} + \varepsilon_2\cot\theta_{2a})}{2},$$
$$\cdots$$
$$W_6 = \frac{(\varepsilon_1\cot\theta_{1b} + \varepsilon_6\cot\theta_{6a})}{2}. \tag{13}$$

The coupling coefficient to a neighboring mesh point depends on the dielectric constants and geometries of the

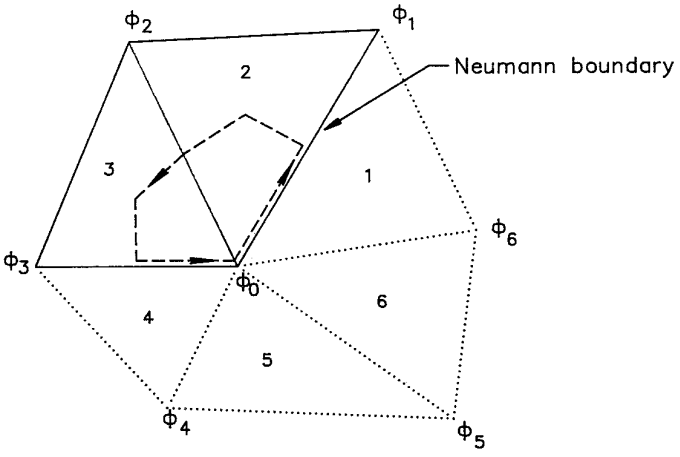

FIG. 4. Gauss's law integration path for a reference mesh vertex on a Neumann boundary. Triangles 2 and 3 are inside the medium, while Triangles 1, 4, 5, and 6 are outside. The Neumann boundary lies on the lines from vertex 3 to 0 and vertex 0 to 1.

triangles on each side of the connecting line. Equation (12) represents a set of coupled linear equations, one for each vertex of the mesh.

A specialized Neumann boundary has the normal derivative of potential equal to zero. This condition implies that the electric field is parallel to the surface. The Neumann boundary, often used to represent symmetry planes in electrostatic problems, is difficult to handle in finite-difference treatments except along straight boundaries. In contrast, the specialized Neumann condition is implicit in the finite-element method [20] for boundaries of any shape. This property can easily be understood from the Gauss's law construction. The result suggests a method to describe arbitrary Hall boundaries, the subject of Section 3. Figure 4 shows a reference point on a specialized Neumann boundary. The active computational region includes two triangles. The other four triangles are outside the boundary. Consider application of Gauss's law over the volume shown to find the relationship between vertex potentials. The volume integral of space charge extends over the two internal triangles. The surface integral of the normal electric field over these triangles proceeds in the same way as the discussion above. There is no contribution over the Neumann surface because the normal electric field is zero by definition. The important point is that the same relationship between the potentials Φ_0, Φ_1, Φ_2, and Φ_3 would result if the surface integral extended over all six surrounding triangles, as long as q_i and ε_i in the external triangles equal zero. From this result, we can identify a convenient way to handle Neumann boundaries in a finite-element code [22]. First, during mesh generation at least one layer of dummy triangles is assigned outside the elements of the computational region. Second, the space charge densities and dielectric constants in the external triangles are set to zero and the external vertices are assigned arbitrary values of potential. Finally, during the solution the potentials at the external vertices are not updated and the Neumann boundary points are treated like any internal point. Thus, there is no need to apply special routines to the boundaries, simplifying the coding task.

3. FINITE-ELEMENT EQUATIONS FOR HALL PROBE REGIONS AND BOUNDARIES

A Hall probe consists of a thin sheet of metal or semiconductor deposited on an insulating substrate. Electrodes on the ends drive a current through the sheet. If there is a component of magnetic field normal to the sheet, the conduction particles feel a transverse force. Charge displacement creates a transverse electric field that allows the particles to travel along approximately straight line paths between the electrodes. Detection of the voltage associated with the transverse electric field gives a measurement of the magnetic field. In this report, the discussion is limited to the Hall equations in the regime discussed in Refs. 1 and 5. An *n*-type material is assumed where minority carrier transport and concentration gradients can be neglected. If variations in the electric and magnetic fields are slow compared with the electron transit time, a steady-state solution is sufficient. In this case, the governing equations are

$$\nabla \cdot \bar{J} = S \tag{14}$$

and

$$\bar{E} = \rho \bar{J} - K_H(\bar{J} \times \bar{B}) = -\nabla \phi. \tag{15}$$

Equation (14) expresses conservation of charge—the quantity S is the source current per volume added or extracted at a point. Equation (15) relates the current density vector to the electric field in the presence of a magnetic field. The quantity ρ is the volume resistivity of the material and K_H is the Hall coefficient, which is a negative number when the majority carriers are electrons. Commercial Hall probes usually have small thickness compared with their transverse dimensions. Therefore, a two-dimensional solution of Eqs. (14) and (15) is adequate. Assuming that the probe lies in the x–y plane and taking B in the z-direction, the component forms for Eq. (15) are

$$\frac{E_x}{\rho} = J_x - \alpha J_y \tag{16}$$

and

$$\frac{E_y}{\rho} = J_y - \alpha J_x,$$

where $\alpha = K_H B/\rho$. Solving for the current density components gives

$$J_x = \frac{E_x + \alpha E_y}{\rho(1+\alpha^2)}, \qquad J_y = \frac{E_y - \alpha E_x}{\rho(1+\alpha^2)}. \tag{17}$$

The finite-element equations for a Hall probe follow from the integral form of Eq. (14) around the closed surface surrounding a sample mesh point shown in Fig. 2. The surface integral of the normal component of **J** around the curve equals one-third of the sum of the current added to the surrounding triangular elements,

$$\sum_{i=1}^{6} \frac{I_i}{3}. \tag{18}$$

There are no injection currents over most of the Hall probe volume. The quantities I_i are useful to represent the effect of circuit loading. Current can be added to or extracted from regions in the solution space that represent sensor contacts.

In the linear approximation, the magnetic field is constant over an element and the potential varies linearly. This implies that the element current density is a constant. We again concentrate on Triangle 2 of Fig. 2. The normal integral of current density is

$$\iint \overline{J}_2 \cdot \overline{n}\, dS = \frac{w_2(\overline{J}_2 \times \overline{L})}{\overline{z}}. \tag{19}$$

Note that the layer height w_2 is an element characteristic. This enables modeling of Hall probes with spatially varying thickness. Substitution of Eqs. (6) and (17) into Eq. (19) gives a relationship for conservation of current in terms of values of the electrostatic potential at the element vertices. The quantities ρ_2 and α_2 are also characteristic of the element, representing the spatial variation of volume resistivity, Hall coefficient, and magnetic field. The right-hand side of Eq. (19) becomes

$$\frac{w_2}{\rho_2(1+\alpha_2^2)}\left[\left[\frac{(y_2-y_1)u}{2} - \frac{(x_2-x_1)v}{2}\right] + \alpha_2\left[\frac{(y_2-y_1)v}{2} - \frac{(x_2-x_1)u}{2}\right]\right]. \tag{20}$$

The first bracketed term has a form similar to those encountered in the Gauss's law treatment of Section 2. It leads to expressions for the coupling coefficient like those of Eq. (13) with the substitution

$$\varepsilon_2 \Rightarrow \gamma_2 = \frac{w_2}{\rho_2(1+\alpha_2^2)}.$$

The effect of a magnetic field is represented by the second bracketed term in Eq. (20). Substituting for u and v from Eq. (7), the term reduces to the simple expression

$$\alpha_2 \frac{\Phi_2 - \Phi_1}{2}. \tag{21}$$

Again, the procedure is to add terms for the six surrounding triangles and to solve for the reference potential Φ_0. The final result can be written as

$$\Phi_0 = \frac{\sum_{i=1}^{6} V_i \Phi_i + \sum_{i=1}^{6} \frac{I_i}{3}}{\sum_{i=1}^{6} W_i}. \tag{22}$$

The coupling coefficients are

$$W_1 = \frac{(\gamma_2 \cot\theta_{2b} + \gamma_1 \cot\theta_{1a})}{2}, \quad \ldots \quad W_6 = \frac{(\gamma_1 \cot\theta_{1b} + \gamma_6 \cot\theta_{6a})}{2}, \tag{23}$$

and

$$V_1 = \frac{(\gamma_2 \cot\theta_{2b} + \gamma_1 \cot\theta_{1a}) + \gamma_2\alpha_2 - \gamma_1\alpha_1)}{2}, \quad \ldots \quad V_6 = \frac{(\gamma_1 \cot\theta_{1b} + \gamma_6 \cot\theta_{6a} + \gamma_1\alpha_1 - \gamma_6\alpha_6)}{2}, \tag{24}$$

Equation (22) applies to internal regions of Hall probes with arbitrary spatial variations of magnetic field, resistivity, Hall coefficient, and thickness. With no modification, the equation also describes generalized Hall boundaries with curvature and variations of medium properties. The treatment parallels that of the specialized Neumann boundary in electrostatics. Here, the condition is that the normal component of **J** is zero along the boundary. A Hall boundary can be implemented simply by surrounding the computational region with a layer of dummy triangles with $\alpha_i = 0$ and $\gamma_i = 0$. In this way, all points are treated as

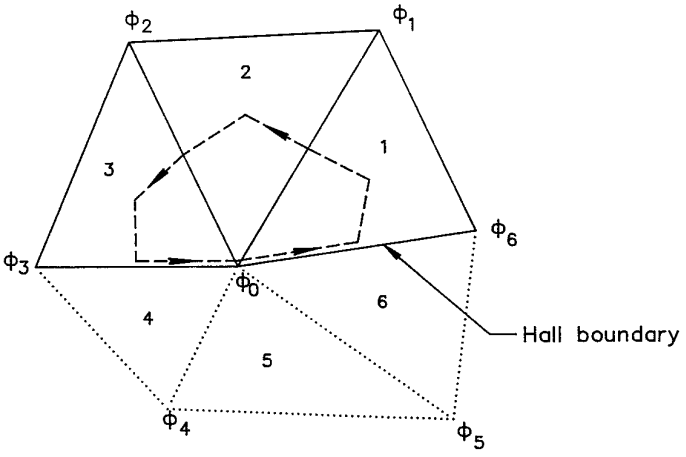

FIG. 5. Integration path for the total current flux away from a reference point on a Hall boundary. Triangles 1, 2, and 3 are part of the probe, while Triangles 4, 5, and 6 are external. The Hall boundary lies on the line from vertex 3 to 0 and vertex 0 to 6.

internal points. The boundaries automatically satisfy Hall conditions unless they are specified as Dirichlet boundaries. In the limit $\alpha \to 0$, a Hall boundary approaches the specialized Neumann condition.

The following construction gives insight into the meaning of Eq. (22). Figure 5 shows a reference point on the Hall boundary of a homogeneous medium. Triangles 1, 2, and 3 are inside the medium while Triangles 4, 5, and 6 are outside. Application of Gauss's law (Eq. (2)) around the dashed line gives an equation that relates Φ_0 to Φ_1, Φ_2, and Φ_3. Because there is no enclosed space charge, the integral of normal electric field equals zero. If the values of α and γ are zero in the external triangles, then we know from the discussion of Section 2 that the integral around the curve in the internal triangles is

$$\Phi_0(W_6 + W_1 + W_2 + W_3) - \Phi_6 W_6 - \Phi_1 W_1 - \Phi_2 W_2 - \Phi_3 W_3.$$

To do the integral along the boundary, note that the condition $J_\perp = 0$ implies that $E_\perp = \alpha E_\parallel$ (Eq. (17)). The integral of parallel electric field from Point a to Point 0 is $(\phi_3 - \phi_0)/2$. Therefore, the integral of normal electric field over the boundary from point a to point b is

$$\int_a^b \overline{E_\perp} \cdot \overline{ds} = \frac{\alpha(\Phi_3 - \Phi_6)}{2}. \tag{25}$$

Gathering all terms in the integral and solving for Φ_0 replicates the result of Eq. (22). For a homogenous medium, terms of the form $(\gamma_{i+1}\alpha_{i+1} - \gamma_i\alpha_i)$ in the expressions for V_i cancel in adjacent triangles except for the points on the boundary, Φ_3 and Φ_6.

4. IMPLEMENTATION IN A NUMERICAL CODE

The method of Eq. (22) was integrated into a numerical package for Hall probes design. The program can handle up to 100,000 triangles. The adaptive mesh generator uses a regular logic where six triangles surround each point. Initially, a rectangular region is filled with triangles with the option for variable resolution along the x and y axes. The region includes an additional peripheral layer so that there is at least one dummy triangle external to each active element. The mesh is initialized so that all vertex points are variable and all elements have $\alpha = 0$ and $\gamma = 0$. The shapes of the probe and electrodes are defined by processing a series of line segments and arcs. Vertex points are moved so that triangle boundaries lie along the curves. Each set of geometric elements defines a *region.* The region number is assigned to vertex points along the boundary. If the region is closed, all internal vertices and elements are marked with the region number. The mesh of Fig. 1 illustrates the procedure. Only active triangles are shown. Region 1 includes the boundary of the Hall probe and the interior elements. Regions 2 and 3 are lines along the left and right sides of the mesh, while Regions 4 and 5 are the top and bottom contact pads. Defining the pad boundary sets the region numbers of enclosed triangles to 4 or 5. After clamping vertices on the region boundaries, the positions of remaining vertices are relaxed to form the smooth mesh of Fig. 1a.

Material properties are defined in the field-solution program. The program assigns constant properties over a re-

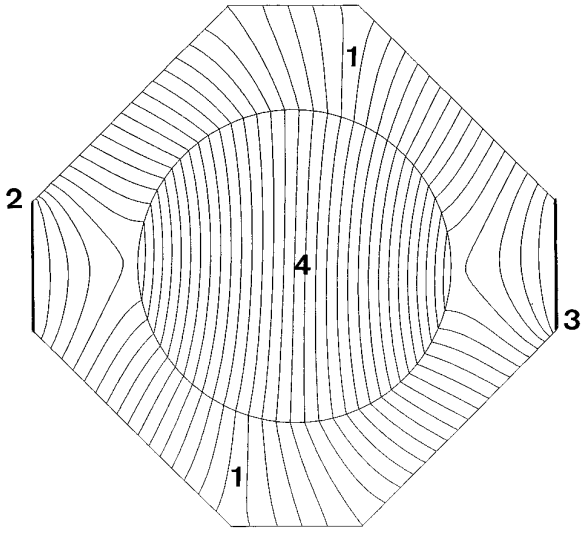

FIG. 6. Equipotential lines (0.25 mV interval) in a Hall probe with an irregular external boundary and internal void. Region 1, conductive material with $K_h = -3.0 \times 10^{-4}$ V·cm/G·A, $\rho = 0.1$ Ω·cm; region 2, fixed potential, 0.0 mV; region 3, fixed potential, 10.0 mV; region 4, void with $\rho = 1000$ Ω·cm.

gion, although it is straightforward to extend the method of Section 3 to continuous variations. For the example, global values of the magnetic field ($B_z = 100$ G) and layer thickness ($w = 1$ μm) are assigned to all triangles. The triangles marked as Region 1 have the parameters $\rho = 0.1$ $\Omega \cdot$ cm and $K_H = -3.0 \times 10^{-4}$ V $\cdot$ cm/G $\cdot$ A. For this choice, $\alpha = 0.3$ and the associated Hall angle is 16.7°. The end regions have constant potentials of 0.0 and 10.0 mV. The potentials of the associated vertices remain unchanged during the relaxation solution. The potentials of the contact pads are not known in advance. Therefore, these regions are modeled as conductors with $\rho = 10^{-4}$ $\Omega \cdot$ cm and $K_H = 0.0$. The relaxation solution brings them to the correct potential so that the integral of current over the pad boundary is zero. The values of W_i and V_i are determined from the element shapes and material properties. The resulting set of equations is solved by successive overrelaxation with Chebyshev acceleration [15, 23]. Figure 1b illustrates equipotential lines of the solution for an open circuit between the contacts. Note that the electric fields intersect the open boundary at the Hall angle, even around the curved extensions. There is a smooth transition to $E_\perp = 0$ at the connection to the drive electrodes. The potential difference between the contacts is 1.042 mV. The total drive current determined by integrating E/ρ over the left electrode surface is 4.1 μA. Finally, Fig. 1c shows how the potential is modified by strong sensor circuit loading. Currents of ± 1.0 μA are assigned to the top and bottom contacts. The current of each triangle in the pad equals the total current multiplied by the ratio of the triangle area to that of the contact. Conservation of current ensures that the integral of current density around the pad boundary equals the total source value. In this case, circuit loading drops the potential between the contacts to 0.618 mV, giving a sensing circuit input impedance of 618 Ω. Finally, Fig. 6 illustrates the ability of the method to handle mixed external boundaries and a curved internal boundary. The Hall angle in the probe material is again 16.7°. There are constant potential contacts at the left and right, while the remaining boundaries are open. The large circle in the center is a void. Note the smooth transition from Dirichlet to Hall boundaries and the preservation of the Hall angle over both the external and internal boundaries.

ACKNOWLEDGMENTS

I thank Joseph P. Heremans of the General Motors Research and Development Center for suggesting this study. I am grateful to the Accelerator Code Group of the Los Alamos National Laboratory for the permission to use algorithms from the Automesh and Lattice programs in the mesh generator. This work was supported by the Field Precision Company.

REFERENCES

1. See, for instance, N. W. Ashcroft and N. D. Mermin, *Solid State Physics* (Saunders, Philadelphia, 1976), p. 11.
2. A. C. Beer, *Solid-State Electron.* **9,** 339 (1966).
3. H. Hollitscher, *Solid-State Electron.* **9,** 581 (1966).
4. H. P. Baltes and R. S. Popvic, *Proc. IEEE* **74,** 1107 (1986).
5. A. Nathan, W. Allegretto, H. P. Baltes, and Y. Sugiyama, *IEEE Trans. Electron Dev.* **34,** 2077 (1987).
6. A. Nathan, W. Allegretto, H. P. Baltes, and Y. Sugiyama, *IEEE Electron Dev. Lett.* **8,** 1 (1987).
7. G. DeMey, *Adv. Electron. Electron Phys.* **61,** 62 (1983).
8. A. M. J. Huiser and H. P. Baltes, *IEEE Electron. Dev. Lett.* **5,** 482 (1984).
9. T. Mimizuka, *Solid-State Elec.* **14,** 107 (1971).
10. R. Chwang, B. J. Smith, and C. J. Crowell, *Solid-State Elec.* **17,** 1271 (1974).
11. A. Nathan, A. M. J. Huiser, and H. P. Baltes, *IEEE Trans. Elec. Dev.* **32,** 1212 (1985).
12. A. W. Baird, *IEEE Trans. Magnetics* **15,** 1138 (1979).
13. M. G. Guvenc, *IEEE Trans. Elec. Dev.* **35,** 1851 (1988).
14. L. Andor, *IEEE Trans. Elec. Dev.* **32,** 1224 (1985).
15. D. Potter, *Computational Physics* (Wiley, New York 1973).
16. K. S. Kunz and R. J. Luebbers, *Finite Difference Time Domain Method for Electromagnetics* (CRC Press, Boca Raton, 1993).
17. M. N. O. Sadiku, *Numerical Techniques in Electromagnetics* (CRC Press, Boca Raton, 1992).
18. C. W. Steele, *Numerical Computation of Electric and Magnetic Fields* (Van Nostrand Reinhold, New York, 1987).
19. R. C. Boonton, *Computational Methods for Electromagnetics and Microwaves* (Wiley, New York, 1992).
20. P. P. Silvester and R. K. Ferrari, *Finite Elements for Electrical Engineers,* 2nd ed., (Cambridge Univ. Press, Cambridge, 1990).
21. A. M. Winslow, *J. Comp. Phys.* **12,** 2149 (1967).
22. Los Alamos Accelerator Code Group, *Reference Manual for the Poisson/Superfish Group of Codes* LA-UR-87-126, (Los Alamos National Laboratory, 1987), unpublished.
23. See, for instance, W. H. Press, S. A. Teukolsky, W. T. Vetterling, and B. R. Flannery, *Numerical Recipes in C,* 2nd ed., (Cambridge University Press, Cambridge, 1992), Sect. 19.5.